Volume 16
Number 6
23 March 2026
Pages 1891–2218

Catalysis Science & Technology

rsc.li/catalysis

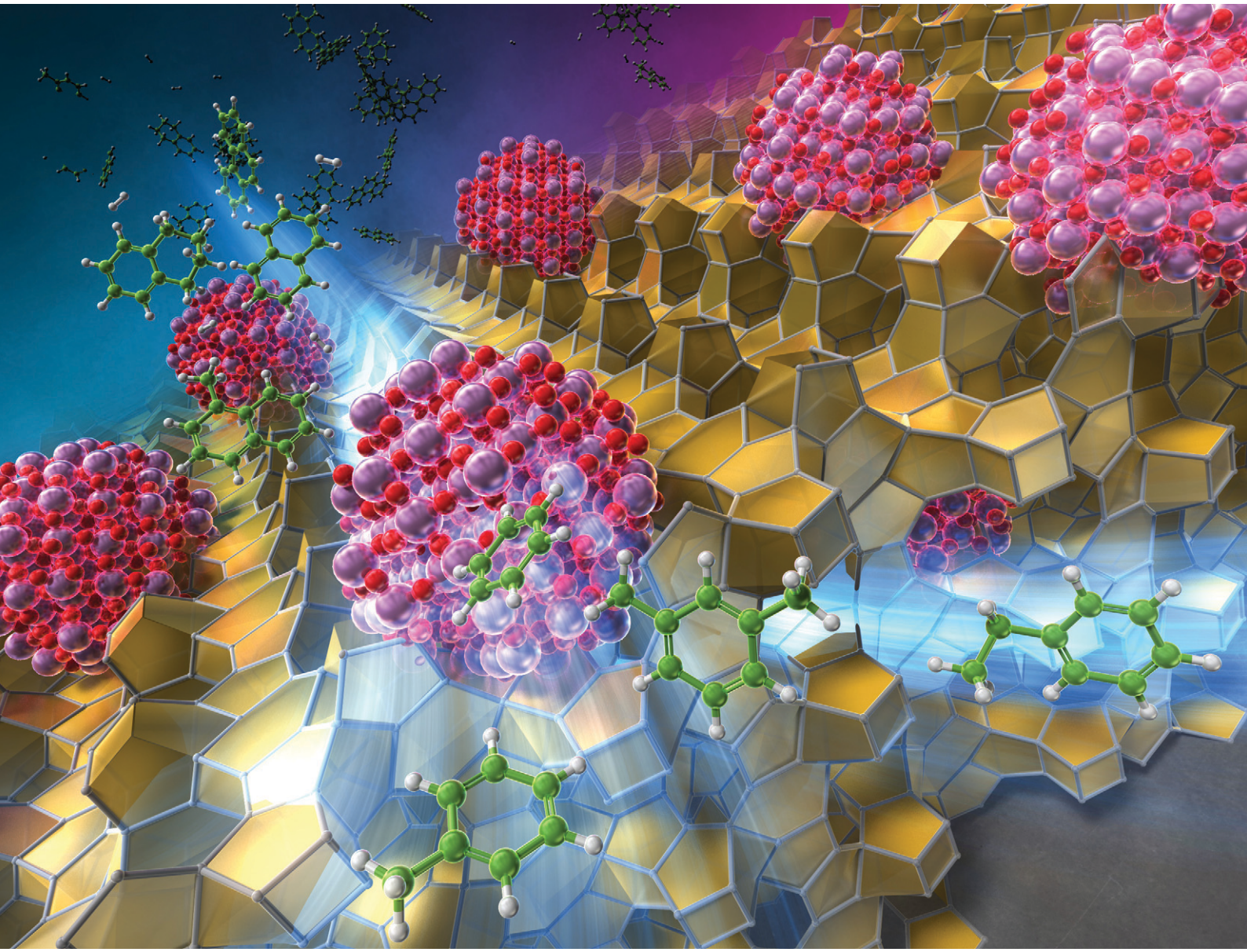

ISSN 2044-4761

ROYAL SOCIETY OF CHEMISTRY

PAPER

Satoshi Suganuma *et al.*

Conversion of polycyclic aromatic hydrocarbons into key monoaromatic hydrocarbons through partial hydrogenation and ring-opening using MoO_x-loaded beta zeolite catalyst

Catalysis Science & Technology

ROYAL SOCIETY OF CHEMISTRY

PAPER

View Article Online
View Journal | View Issue

Cite this: *Catal. Sci. Technol.*, 2026, **16**, 1925

Conversion of polycyclic aromatic hydrocarbons into key monoaromatic hydrocarbons through partial hydrogenation and ring-opening using MoO_x-loaded beta zeolite catalyst

Satoshi Suganuma, *[a] Sayaka Sekino,[b] Kazuki Nakajima,[b] Kazu Okumura,[c] Etsushi Tsuji[b] and Naonobu Katada[b]

This study demonstrates an efficient method for converting polycyclic aromatic hydrocarbons (PAHs) into key monoaromatic hydrocarbons (BTEX: benzene, toluene, ethylbenzene, and xylenes) *via* partial hydrogenation and ring-opening reactions using MoO_x nanocluster-loaded beta zeolite catalysts. The catalysts were prepared with various Mo loadings (1–20 wt%) and characterized by XRD, HAADF-STEM, N_2 adsorption, FTIR, NH_3 IRMS-TPD, and XAFS to elucidate Mo dispersion, oxidation states, and acid properties. At optimal Mo loading (10 wt%), MoO_x nanoclusters located mainly on external defect sites synergistically interacted with Brønsted acid sites on beta zeolite, activating H_2 molecules and promoting selective BTEX formation in tetralin conversion while suppressing side reactions such as ring contraction to methylindane and dehydrogenation to naphthalene. Conversion of 1-methylnaphthalene, naphthalene, and phenanthrene under high H_2 pressures revealed that MoO_x nanoclusters facilitated partial hydrogenation to tetralin derivatives, followed by mainly acid-catalyzed ring opening to BTEX. The higher BTEX yield from a mixture of 1-methylnaphthalene and naphthalene achieved 52.8 C-mol%. Although phenanthrene conversion was less efficient due to hydrogenation limitations, the results suggest the potential of MoO_x/beta zeolite as a non-precious-metal catalyst system for PAH valorization. This work provides the first detailed structural–activity relationship for MoO_x/beta zeolite catalysts in high-yield BTEX production from PAHs.

Received 29th October 2025,
Accepted 4th February 2026

DOI: 10.1039/d5cy01293g

rsc.li/catalysis

1. Introduction

Hydrocarbons obtained from petroleum are still used worldwide as fuels and as raw materials for chemical products, and they are an indispensable resource for humankind. Therefore, it is necessary to increase their utilization rate until next-generation resources become widely available. In the petroleum refining process, the residue obtained from atmospheric distillation is called atmospheric residue (AR). Even Middle Eastern crude oil, which is rich in low-boiling-point components and is commonly used, produces about 50% AR. When AR is vacuum distilled, about 50% is converted to vacuum gas oil (VGO). VGO is further converted into various petroleum products through fluid catalytic cracking (FCC) or hydrocracking.[1–3] The FCC process produces monocyclic aromatics and olefins, but light cycle oil (LCO) is also produced as a byproduct.[4] LCO contains 20–28% paraffins, 15–17% monocyclic aromatics, 35–55% bicyclic aromatics, and 6–16% polycyclic aromatics with three or more rings.[4] LCO has a boiling point like that of light oil fractions. While it can be used as boiler fuel, its high aromatic content results in a low cetane number, making it difficult to use as diesel fuel and limiting its utilization efficiency. Additionally, the presence of sulfur and nitrogen compounds is another major hurdle. Stringent environmental legislation restricts blending high-sulfur-containing steam into cleaner transportation fuels. If LCO could be converted into BTEX (benzene, toluene, ethylbenzene, and xylenes), it could be used as a raw material for chemicals or gasoline, thereby improving overall petroleum utilization efficiency. Therefore, some researchers have reported studies on producing monocyclic aromatics from LCO.[5] On the other hand, we have researched the novel VGO conversion process

[a] *Institute for Catalysis, Hokkaido University, Kita 21 Nishi 10, Kita-ku, Sapporo 001-0021, Japan. E-mail: suganuma@cat.hokudai.ac.jp; Tel: +81 11 706 9131*
[b] *Center for Research on Green Sustainable Chemistry, Tottori University, 4-101 Koyama-cho Minami, Tottori 680-8552, Japan*
[c] *Department of Applied Chemistry, School of Advanced Engineering, Kogakuin University, 2665-1 Nakano-machi Hachioji-city, Tokyo 192-0015, Japan*

as an alternative to FCC and hydrocracking, which utilizes the dealkylation of alkyl polycyclic aromatic hydrocarbons.[6–9] In this process, the key to improving utilization efficiency also lies in whether alkyl polycyclic aromatic hydrocarbons without side chains can be converted to BTEX.

The conventional method for converting polycyclic aromatics like naphthalene, which are most abundant in LCO, involves hydrocracking in high-pressure H_2 to convert them into naphthenes and paraffins, followed by catalytic reforming to dehydrogenate naphthenes and cyclize paraffins, thereby converting them into BTEX[4,10–14] (Scheme 1). However, since hydrogenation and catalytic reforming are performed in two steps, energy consumption is high, and excessive cracking leads to low-molecular-weight products, resulting in low final BTEX yields. Additionally, catalytic reforming uses costly platinum catalysts. If bicyclic aromatics can be partially hydrogenated to form tetralin compounds, which are then converted into BTEX *via* ring-opening, a new process with reduced energy consumption can be established (Scheme 1). A recent review summarizing reports on BTX production *via* modified conventional hydrogenolysis has been published.[15]

Partial hydrogenation of naphthalene into tetralin requires high-pressure hydrogen due to equilibrium constraints. This makes laboratory-scale flow reactions difficult, limiting knowledge. It is known that partial hydrogenation of naphthalene proceeds on Mo-loaded catalysts,[16–20] whereas using other metal-supported catalysts, such as Ni, Co, or Pt, results in complete hydrogenation, producing decalin.[12,21] When using a Mo_2C-loaded γ-Al_2O_3 catalyst, >99% of tetralin yield has been reported.[22] On the other hand, tetralin conversion using zeolite catalysts results in low yields of benzene derivatives due to the complex interplay among ring-opening, ring-contraction, hydrogenation, and dehydrogenation reactions.[23–26] We have clarified the relationship between the structural characteristics of solid acid catalysts and their catalytic activity in this reaction. We found that beta zeolite, which has strong Brønsted acid sites in the large pores of 12-ring zeolites, exhibits relatively high BTEX yields. Still, the combined yield of the byproducts methylindane and naphthalene was higher than the BTEX yield.[27] In this study, to improve the BTEX yield, we loaded a metal species that promotes hydrogenation on beta zeolite. Precious metals exhibit high activity in various hydrogenation and dehydrogenation reactions, but hydrogenolysis as a side reaction also occurs. Therefore, we investigated the loading of different transition metals (Fe, Ni, Co, and Mo) that possess mild hydrogenation catalysis. The other group reported that a catalyst with Ni_2P supported on beta zeolite produced a 42% BTX yield from 1-methylnaphthalene.[14] Additionally, it has been reported that BTEX was produced with a 40% yield using a catalyst containing Ni and W supported on beta zeolite.[28] To our knowledge, while combinations of molybdenum oxide alone and zeolite have been used in applications such as methane conversion and cellulose decomposition,[29,30] reports of this combination exhibiting high activity in producing BTEX from PAHs are limited. Our catalyst yields higher product yields than Ni_2P- and NiW-supported beta zeolite catalysts[14,28] in the reaction with 1-methylnaphthalene. Furthermore, we also achieved excellent results in activity evaluations using less reactive naphthalene and phenanthrene. We have found that Mo oxides supported on beta zeolite work synergistically with the zeolite's Brønsted acid sites in tetralin conversion and function in the partial hydrogenation of naphthalene. This paper describes the structural analysis of Mo species supported on beta zeolite, followed by the reactions to produce BTEX from tetralin, 1-methylnaphthalene, naphthalene, and phenanthrene. 1-Methylnaphthalene and naphthalene are converted to 5-methyl tetralin and tetralin, respectively, by partial hydrogenation (Scheme S1). If the naphthenic ring of tetralin products is cleaved, BTEX is formed by dealkylation and cracking. If not cleaved, isomerization and hydrogenation form byproducts such as

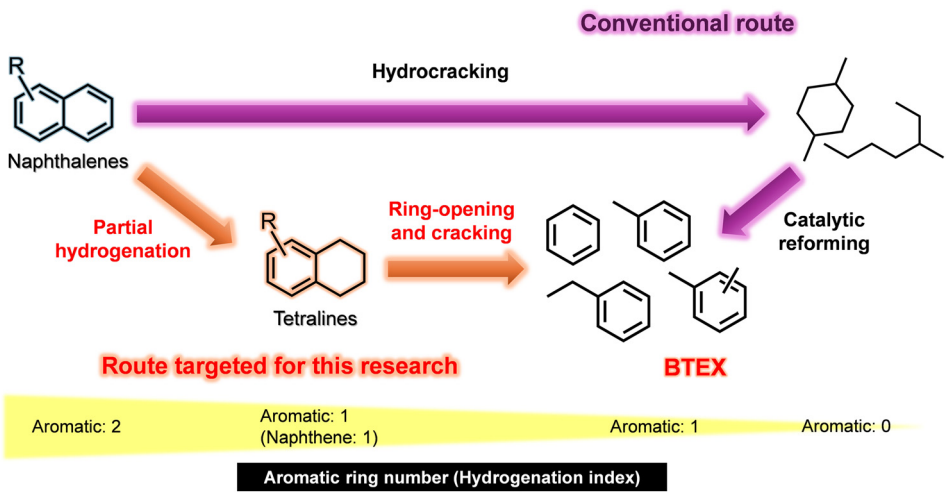

Scheme 1 Route targeted for the efficient BTEX production from naphthalenes.

indane and decahydronaphthalene (decalin). Phenanthrene is assumed to undergo a similar reaction pathway. To understand the effect of Mo loading on suppressing these side reactions, the evaluation of the tetralin conversion is described first, followed by the conversions of polycyclic aromatic hydrocarbons.

2. Experimental

2.1. Catalyst preparation

The beta zeolite (Si/Al_2 = 28, Tosoh, HSZ-930NHA) was heated at 773 K in air for 4 h to remove any remaining OSDA, and then the H-form of beta was obtained. To achieve a Mo loading of 1–20 wt%, $(NH_4)_6Mo_7O_{24}{\cdot}4H_2O$ was dissolved in 100 mL of ion-exchanged water. 2.0 g of beta was added to this solution, which was then evaporated to dryness and dried at 110 °C overnight. The sample was calcined in a muffle furnace at 5 °C min^{-1} to 500 °C for 4 h and is denoted as *X*-Mo (*X* = loading amount).

2.2. Catalyst characterization

The crystalline phases of the catalysts were analyzed by X-ray diffraction (XRD; Rigaku Ultima IV diffractometer) using CuKα radiation over the 2θ range of 5–40°. Cs-corrected scanning transmission electron microscope images of 5-Mo, 10-Mo, and 20-Mo with elemental maps were collected at 200 kV using a Titan3 G2 60-300 (FEI Company) instrument equipped with an energy-dispersive X-ray spectroscopy (EDX) detector. The nitrogen adsorption isotherm was measured at 77 K using a BELSORP-max instrument (Microtrac-BEL) after pretreatment at 573 K for 1 h under vacuum. The volume of liquid nitrogen condensed at $P/P_0 \approx 0.005$ to fill the micropores was calculated as a reference to the micropore volume, using the numerical expression reported in the previous report.[27] Fourier-transform infrared (FTIR) analysis of hydroxy groups on the catalysts was performed by using an IR spectrometer (FT/IR-4200, JASCO). The catalyst powder was compressed at 20 MPa into a self-supporting disk (1 cm in diameter), which was then set in the *in situ* IR cell. The sample was heated to 823 K for 1 h in an H_2 flow (34 μmol s^{-1}). After evacuation, the sample was cooled to 343 K in a He flow (34 μmol s^{-1}). The IR spectrum was recorded in helium flow. The amount and strength of Brønsted sites were analyzed by the NH_3 IRMS-TPD method.[31] A self-supporting disc (1 cm diameter) was molded from the sample by compression, held in a set of metal rings, and fixed in a cell of the Microtrac-BEL IRMS-TPD analyzer. The sample was pretreated at 823 K for 1 h in hydrogen flow (34 μmol s^{-1}). After evacuation, the sample was cooled to 343 K under vacuum. IR reference spectra as $N(T)$ were collected once at 1 K, with the sample heated in a helium flow (68 μmol s^{-1}, 6 kPa) at 2 K min^{-1}. The ammonia was adsorbed at 13 kPa and 343 K, then evacuated for 30 minutes. After being kept in a helium flow at 343 K for 3 hours, the sample was heated under the same conditions as well as before adsorption. At this time, the IR spectra of adsorbed ammonia and the MS response were measured. The difference spectra were calculated as $A(T) - N(T)$. The ammonia TPD profile for the Brønsted acid sites was analyzed as described in our previous study.[32] The amount of acid sites was calculated from the peak intensity in the TPD profile, and the distribution of the enthalpy of ammonia desorption (the so-called adsorption heat) was analyzed by curve fitting. Mo K-edge XAFS measurements[33] were performed at the NW10A beamline with the approval of the Photon Factory in the High Energy Accelerator Research Organization (KEK-PF-AR, Proposal No. 2022G581). The data were acquired in 3 minutes using a Si(311) monochromator in quick scan mode. After the pretreatment of the catalysts in a H_2 flow (50 mL min^{-1}) at 823 K for 1 hour, measurements were performed using a transmission method with ion chambers filled with Ar and Kr for I_0 and I, respectively. Beam size at the sample position was 1.7 mm (horizontal) × 0.8 mm (vertical). X-ray photoelectron spectroscopy (XPS) was performed on a JEOL JPC-9010MC instrument, after the pretreatment of the catalysts in a H_2 flow (50 mL min^{-1}) at 823 K for 1 hour.

2.3. Catalytic reactions for BTEX production

The catalytic reactions were performed under high hydrogen pressure conditions using a fixed-bed flow reactor.[27] Unless otherwise specified, the following reaction conditions were used. 0.20 g of the catalyst was placed in a stainless tube with an inner diameter of 4 mm and then pretreated at 823 K for 1 h in a flow of H_2 (134 mmol h^{-1}). The flow rate of reactants [tetralin, 1-methylnaphthalene (Tokyo Chemical Industry), naphthalene, or phenanthrene (FUJIFILM Wako Pure Chemical Corp.)] was 14.5–16.6 mmol h^{-1}, corresponding to $W_{cat}/F_{reactant}$ = 12–14 g h mol^{-1} at 723 K, whereas that of H_2 was 134–268 mmol h^{-1}. The total pressure in the reactor was maintained at 4.0–5.0 MPa using a back pressure valve. The outlet effluents were trapped in a glass tube at 273 K and analyzed using a gas chromatograph (GC-2014, Shimadzu) with a flame ionization detector and a capillary column (InertCap1, 5.0 μm thickness, 30 m in length, and an internal diameter of 0.53 mm). Untrapped gas products and undetected products by GC, such as deposited hydrocarbons on the catalysts, were defined as others. The conversion and yield were calculated according to the following equations.

$$\text{Conversion} = 1 - \frac{\text{Rate of reactant recovery [mol s}^{-1}\text{]}}{\text{Rate of reactant feed [mol s}^{-1}\text{]}}$$

$$\text{Yield} = \frac{\text{Rate of product formation [mol s}^{-1}\text{]}}{\text{Rate of reactant feed [mol s}^{-1}\text{]}}$$

3. Results

3.1. Structural characteristics of the prepared catalysts

The crystal structures and texture properties were evaluated initially. Fig. 1 shows XRD patterns of the Mo-loaded beta zeolites. The crystal structure of beta zeolite remains in all

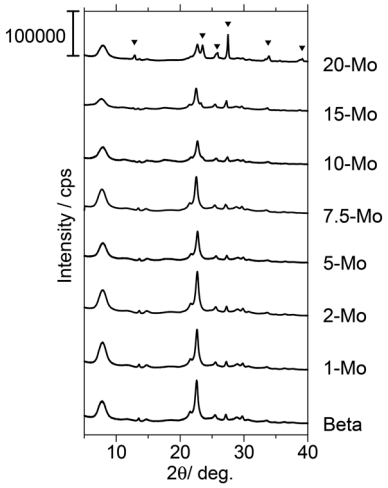

Fig. 1 XRD patterns of Mo-loaded beta zeolite catalysts.

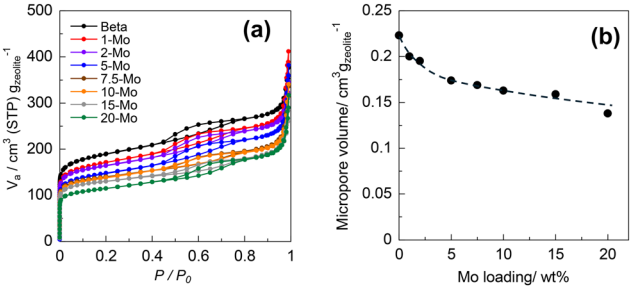

Fig. 3 (a) N_2 adsorption–desorption isotherms of Mo-loaded beta zeolite catalysts and (b) influence of Mo loading on microporous volume.

the catalysts. It appears to disperse the Mo species across almost all the catalysts, as evidenced by the absence of Mo diffraction. On the other hand, 20-Mo (20 wt% Mo-contained catalyst) included the diffraction pattern of α-MoO_3 (PDF 00-005-0508), indicating that the aggregated Mo oxides existed on the external surface of the zeolite. This result is consistent with the literature,[34,35] which shows MoO_3 diffraction peaks at high Mo loading. Fig. 2 displays a high-resolution HAADF-STEM. The white portions indicate the presence of Mo. In 5-Mo and 10-Mo, it appears that Mo nanoclusters (1–2 nm) were dispersed on the outer surface of the zeolite. Mo species on the 20-Mo were widely distributed on the outer surface, and some particles were aggregated, as shown in the line-scan analysis (Fig. S1). The porous structure of the prepared catalysts was evaluated from the nitrogen adsorption–desorption isotherm, which was determined by the N_2 adsorption amount per unit weight of zeolite, to investigate the effect of Mo loading on the microporous structure (Fig. 3(a)). All isotherms exhibit type IV behavior,[36] and the hysteresis loop does not change significantly with Mo loading. On the other hand, the adsorption amount at extremely low pressures ($P/P_0 < 0.005$) decreases with gradually increasing Mo loading. Fig. 3(b) shows the change in microporous volume with Mo loading. Since the micropore volume was significantly reduced up to 5 wt%, it is suggested that Mo fills the pores. Above 5 wt%, the decrease is gradual, implying that Mo is supported on the zeolite's outer surface. Fig. 4 indicates the IR spectra of hydroxyl groups on the beta zeolites after Mo loading. A main peak at 3745 cm^{-1} was found along with a shoulder peak at around 3735 cm^{-1}. The former is attributed to silanol groups present in large lattice defects on the external surface of microcrystalline zeolite, whereas the latter is attributed to silanol groups in small lattice defects on the internal surface.[37,38] The 3608 cm^{-1} band is assigned to strongly acidic bridging Si(OH)Al groups.[37,38] In the case of 1 wt% of Mo loading, the proportion of the acidic OH groups decreased significantly, indicating that Mo was grafted at such acid sites. When the loading amount exceeds 5 wt%, the amount of external silanol groups decreases significantly, indicating that Mo species mainly reside on large defect sites on the external surface.

Brønsted acid sites (BAS) on beta zeolite acted as the active sites for BTEX production from tetralin.[27] In contrast, it is expected that the Mo species will activate the H_2 molecule.

NH_3 IRMS-TPD can be used to evaluate the Brønsted acid sites on the prepared catalysts.[31] This measurement method is reasonable for assessing acidity, since pyridine is larger than NH_3, making it difficult to evaluate acidity throughout the entire zeolite pore structure. Fig. S2 illustrates the difference in IR spectra obtained on the catalysts during the NH_3-TPD (temperature-programmed desorption). A sharp band at *ca.* 1450 cm^{-1} and a small peak at 1250–1330 cm^{-1} were assigned to the bending (ν_4) vibration of NH_4^+ adsorbed on the BAS and bending (δ_s) vibration of NH_3 adsorbed on

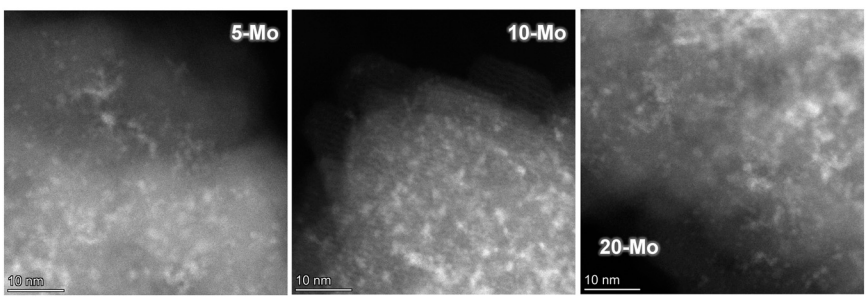

Fig. 2 High-resolution HAADF-STEM images.

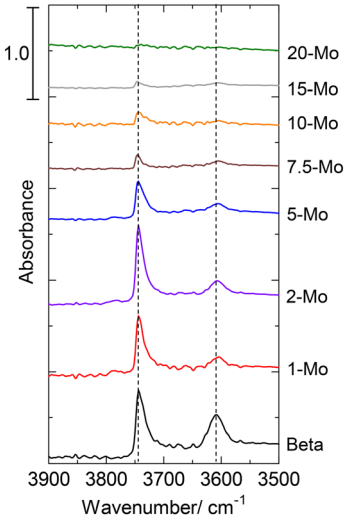

Fig. 4 FTIR spectra of Mo-loaded beta zeolite catalysts.

the Lewis acid sites (LAS), respectively. Fig. S3 shows the TPD profiles of ammonia desorbed from the acid sites; the MS (mass spectroscopy)-TPD is the profile of NH_3 desorption, and the IR-TPD is the profile calculated from the BAS- and LAS-band. We previously reported the influence of acid properties on the conversion of tetralin under pressurized hydrogen conditions.[27] When BAS were present, the naphthenes in tetralin underwent ring-opening and cracking to produce BTEX. Conversely, LAS could dehydrogenate tetralin, yielding naphthalene. This paper focuses on the influence of BAS, which are deeply involved in the target reaction. The enthalpy (ΔH) of NH_3 desorption from the catalysts can be used as an index of acid strength.[31] The strength distributions of Brønsted acid (ΔH_{BAS}) were calculated from the IR-TPD of the BAS band (Fig. S4). Since BAS (>120 kJ mol^{-1}) decreases with Mo loading, it was assumed to be the BAS on the zeolite, while BAS (<120 kJ mol^{-1}), with the opposite tendency, was speculated to be the BAS on Mo oxide. Several papers have reported that supported Mo oxides possess Brønsted acid sites.[39,40] Fig. 5 represents changes in the BASs on the zeolite

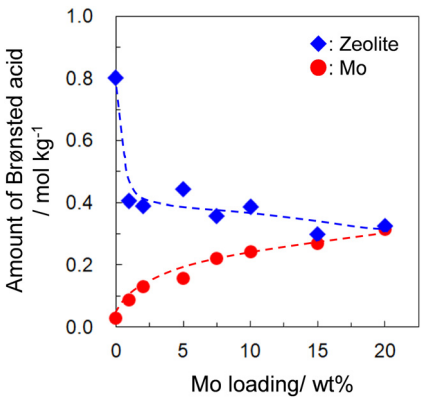

Fig. 5 Influence of Mo loading on the amount of Brønsted acid sites for Mo-loaded beta zeolite catalysts after the pretreatment in H_2 flow at 823 K.

and Mo oxide for each Mo loading. The BAS on the zeolite decreased significantly by 1 wt% Mo loading and then decreased slightly with further Mo loading. On the other hand, the BAS on Mo oxide increased with Mo loading. As reported previously,[27] the strong BAS on the zeolite played a significant role in tetralin conversion. Given the minimal influence of the weak BAS on Mo oxide, we can focus on the BAS on the zeolite.

Mo species might act as a promoter of tetralin conversion to BTEX and as an active site for the partial hydrogenation of naphthalene. It is crucial to analyze the Mo oxidation states to understand these effects. XAFS analysis was conducted to characterize Mo species. XANES spectra of the Mo K-edge were collected after the reduction of the Mo-loaded zeolite catalysts in flowing H_2 gas at 823 K (Fig. 6(a) and (b)). This pretreatment should reduce the MoO_3 content in the 20-Mo observed in the XRD measurement. The spectra of MoO_3, MoO_2, and Mo_2C were observed as standards. It is known that the absorption edge shifts to lower energy as the oxidation state of Mo decreases.[41,42] The major Mo species on 10-Mo can be attributed to a slight reduction from MoO_2. The oxidation states of 1-Mo, 5-Mo, 10-Mo, and 20-Mo were estimated by comparing the Mo K-edge energies to a linear fit of the K-edge energies for the standards (Fig. S5). Increased Mo loading was found to gradually decrease the oxidation state, *i.e.*, from +4.0 to +2.3 (Fig. 6(c)). Fig. S6 represents (a) EXAFS and (b) FT-EXAFS spectra. Mo–O at ≈1.6 Å and Mo–Mo at ≈2.6 Å were observed in the spectra for 5-Mo and 10-Mo; the primary species present was identified as MoO_2. In 20-Mo, the Mo–Mo peak was observed at ≈2.4 Å, larger than elsewhere, indicating a higher Mo metal content. The XPS technique was also employed (Fig. S7). As for the Mo 3d spectra, doublet peaks can be observed and assigned to $3d_{5/2}$ (Mo: 228.0, Mo^{4+}: 229.5, Mo^{5+}: 231.2, and Mo^{6+}: 232.7 eV) and $3d_{3/2}$ (Mo: 231.3, Mo^{4+}: 232.8, Mo^{5+}: 234.5, and Mo^{6+}: 236.0 eV). The amounts of Mo^{4+} and Mo species increased with increasing Mo loading. This is consistent with the XAFS results, indicating that the majority of Mo species are present on the zeolite surface. However, several peak positions overlap, making it difficult to separate them and accurately estimate the distribution. The oxidized Mo(VI) should have formed on beta zeolite during catalyst preparation by calcination in air, suggesting that hydrogen reduction occurred during pretreatment. The Mo species on 1-Mo is presumed to contain grafted Mo(VI)-oxo at BAS[43] and then reduced to exist as Mo(IV) within the micropores. When the loading amount exceeded 5 wt%, it is speculated that Mo nanoclusters in large defect sites on the external surface were reduced from MoO_3 to MoO_2, and the surface of the MoO_2 nanoclusters was reduced.

3.2. BTEX production from tetralin, 1-methyl naphthalene, naphthalene, and phenanthrene

The 5 wt% of metal loading effect on beta zeolite was briefly screened under the same reaction conditions (623 K) as in a

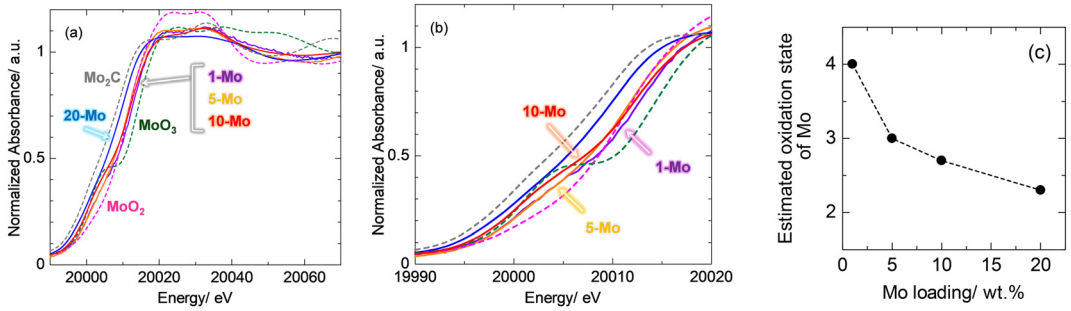

Fig. 6 Mo K-edge XANES spectra of standard samples (dashed line) and Mo-loaded beta zeolite catalysts after the pretreatment in H_2 flow at 823 K (solid line) using X-ray absorption spectroscopic analysis. (a) Wide range (19 990–20 070 eV), (b) narrow range (19 990–20 020 eV), and (c) correlation between Mo loading and oxidation state.

previous report on tetralin conversion using H^+-type zeolite[27] (Fig. 7). Loading Fe and Co decreased conversion in comparison with H^+-type beta zeolite (catalyst name: none). Ni loading increased conversion, but the yield of the desired products remained almost unchanged, and the products with completely hydrogenated aromatic rings (cyclohexanes and decalin) increased. Only Mo loading increased the BTEX yield without excessive hydrogenation. The effect of Mo loading on conversion and product yields was then investigated at a higher temperature (723 K) (Fig. 8(a)). The BTEX yield steadily increased with increasing Mo loading and conversion. 10-Mo exhibited 62.0% of BTEX yield, whereas the yields of methylindane and naphthalene gradually decreased, showing 4.8% and 6.6% in 10-Mo, respectively. Since a portion of the outlet effluents was not trapped and was exhausted as a gaseous component, it was collected using a gas collector. The gas yields for C3 and C4 were 9.2% and 7.4%, respectively. These were probably produced from tetralin together with toluene and benzene. Increasing the Mo loading further decreased the BTEX yield and increased the yields of methylindane and naphthalene. The effect of H_2 partial pressure on the reaction rate was investigated using 1-Mo and 10-Mo (Fig. 8(b)). The formation rates of BTEX (V [mmol h^{-1} g^{-1}]) increased with increasing H_2 pressure for both catalysts. From the slopes of the straight lines, the reaction orders for H_2 pressure were calculated to be +1.1 and +1.9 for 1-Mo and 10-Mo, respectively. These results indicate that the reaction order increased with increasing Mo loading. It is evident that H_2 and Mo strongly influence the rate-limiting step in BTEX formation from tetralin.

It has been reported that partial hydrogenation of naphthalene proceeds using a Mo-loaded catalyst.[16–20] In this paper, the Mo species on beta zeolite was suggested to activate hydrogen molecules in tetralin conversion, and hydrogenation of the aromatic ring of naphthalene could also be expected. First, catalytic reactions were conducted to produce BTEX from 1-methylnaphthalene (1-MN), as shown in Table 1. Beta zeolite without Mo species showed high conversion, but the main product was 2-methylnaphthalene (2-MN) formed by isomerization of 1-MN. Hydrogenation of aromatic rings in naphthalene hardly proceeded on beta zeolite. In comparison, 10-Mo exhibited higher conversion and BTEX yield than beta zeolite. It is thought that Mo species formed tetralin derivatives through partial hydrogenation of 1-MN, and that the BAS and Mo on beta zeolite produced BTEX through ring opening and cracking of the naphthenic ring in tetralin derivatives. Second, the reaction was performed under conditions where naphthalene and 1-MN were supplied. Since it is experimentally challenging to perform the reaction with flowing solid

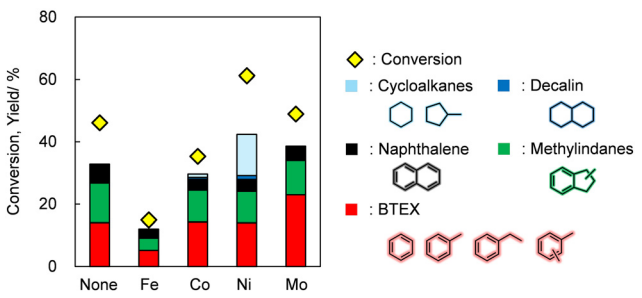

Fig. 7 Conversion and product yields averaged between 3 and 5 h in tetralin conversion over metal (5 wt%)-loaded zeolites. Reaction conditions: catalyst 0.20 g, $W_{cat}/F_{tetralin}$ 12 g h mol^{-1}, reaction temperature 623 K, H_2 flow 134 mmol h^{-1}, and total pressure 4.0 MPa.

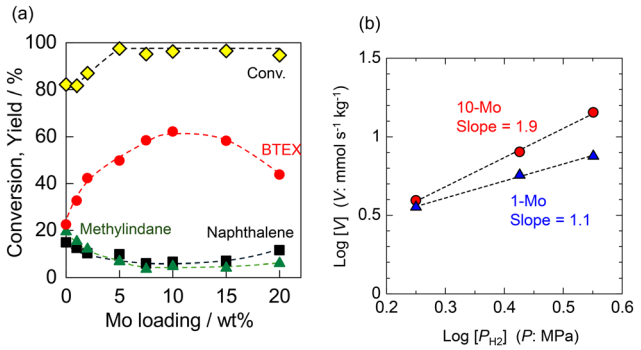

Fig. 8 (a) Influence of Mo loading on conversion and product yields averaged between 3 and 5 h in tetralin conversion over Mo-loaded beta zeolite and (b) BTEX formation rates (V) as a logarithmic function of H_2 pressure in tetralin conversion on representative Mo-loaded beta zeolite catalysts with 1 and 10 wt% Mo. Reaction conditions: catalyst 0.20 g, $W_{cat}/F_{tetralin}$ 12 g h mol^{-1}, reaction temperature 723 K, H_2 flow 134 mmol h^{-1}, and total pressure (a) 4.0 MPa and (b) 2.0–4.0 MPa.

Table 1 BTEX production from polycyclic aromatic hydrocarbons (1-MN: 1-methyl naphthalene, Np: naphthalene, and Pnt: phenanthrene). Conversion and product yields averaged between 3 and 5 h; reaction conditions: catalyst 0.20 g, reaction temperature 723 K, and H_2 flow 134 mmol h^{-1}

Reactant	Catalyst	Press./MPa	$W_{cat}/F_{reactant}$/g h mol^{-1}	Conv./%		Yield/C-mol%			
				1-MN	Np or Pnt	BTEX	Nps	Indanes	Tetralins
1-MN	Beta	4.0	13	74.7	—	1.7	63.8[a]	0	0.3
	10-Mo	4.0	13	96.7	—	46.3	21.3[a]	0.3	0
1-MN/Np = 3	10-Mo	4.0	13	88.5	42.4	27.6	31.9[b]	0.7	0.5
	10-Mo	5.0	13	99.0	95.3	52.8	4.4[b]	0	0
1-MN/Pnt = 4	10-Mo	5.0	14	86.6	55.4	15.3	53.4[b]	0.4	0.1

[a] Yield of naphthalene, 2-MN, and dimethyl naphthalene. [b] Yield of 2-MN and dimethyl naphthalene.

naphthalene, the reaction was carried out by dissolving naphthalene in 1-MN (1-MN/naphthalene (Np) = 3). Compared to when only 1-MN was provided, the BTEX yield decreased, and the yield of two-ring aromatic compounds (Nps) increased. This was attributed to the lower hydrogenation rate of naphthalene. In addition, a small amount of indanes and tetralins was produced, indicating that the BTEX production rate in the subsequent reaction decreased. When the hydrogen pressure increased from 4 to 5 MPa, the Np conversion and BTEX yield improved. The components of BTEX are as follows: benzene 19.6%, toluene 48.9%, ethylbenzene 5.4% and xylenes 26.1%. In addition, indanes and tetralins were below the detection limit. The BTEX production resulted in the formation of byproducts of C1–C4 hydrocarbons: C1 3.9%, C2 6.0%, C3 21.9%, and C4 13.3%. The increase in hydrogen pressure accelerated the reaction rates of hydrogenation in the former and BTEX production in the latter. The reaction with flowing phenanthrene and 1-MN was carried out under the same conditions as naphthalene and 1-MN. Unfortunately, the BTEX yield decreased significantly, while the Nps yield increased. The presence of phenanthrene decreased the hydrogenation rate of the polycyclic aromatic hydrocarbons. It is essential to perform the reaction at higher hydrogen pressures; however, this is not possible due to the equipment's maximum safe pressure of 5 MPa. However, the possibility of BTEX formation from polycyclic aromatic hydrocarbons with three or more rings remains.

4. Discussion

It was expected that the BAS of beta zeolite and Mo species would work synergistically in the conversion of tetralin and polycyclic aromatic hydrocarbons. Understanding the Mo properties helps clarify this effect. The Mo location information on beta zeolite was obtained from XRD (Fig. 1), HAADF-STEM (Fig. 2), and N_2 adsorption measurements (Fig. 3). At Mo loadings of 5 wt% or less, most of the Mo species existed in the micropores, with some loading outside the micropores. At the higher loading amounts, Mo was increasingly supported on the surface outside the micropores, and nanoclusters of several nanometers were dispersed. Since no Mo diffraction appeared in XRD, the MoO_x nanoclusters were smaller than 5 nm. Previous literature reported Mo oxides supported on beta zeolite to be 2.5–3.5 nm in size, suggesting a similar size is possible.[44] Clear diffraction appeared in 20-Mo of XRD, indicating the presence of large crystal particles. The Mo location can be inferred from IR changes in the zeolite's OH groups (Fig. 4). Mo nanoclusters are grafted onto the zeolite's acidic OH groups at low loading levels. As loading increases, they are mainly loaded onto silanol groups at lattice defects on the zeolite's external surface. In evaluating acidity, the BAS on the zeolite decreased with Mo loading. At the same time, the BAS on Mo oxide increased with Mo loading (Fig. 5). The supported Mo species are largely reduced from MoO_3, but, as indicated by XPS (Fig. S7), some residual Mo^{6+} species may be involved in BAS formation.[45] We have already reported that the strong BAS on the zeolite played a role in the tetralin conversion.[27] Given the minimal influence of the weak BAS on Mo oxide, we can focus on the BAS on the zeolite. The Mo oxidation state could be determined from XAFS measurements (Fig. 6). The Mo loading amount decreased the oxidation state from +4.0 (on 1-Mo) to +2.3 (on 20-Mo). The pretreatment at 823 K should reduce Mo species to MoO_2 and further reduce some of it to Mo.[46] As the Mo nanoclusters on beta zeolite became larger, the stabilization effect by grafting on the OH groups of the zeolite decreased, and some of the MoO_2 may have been reduced to Mo. The Mo oxides are commonly used as catalyst components in reduction reactions. This behavior extracts hydrogen from H_2 molecules, stabilizes the hydride on the Mo species, and allows BAS to accept the corresponding proton.[47] Several previous studies have reported that Mo dimers in zeolite pores are active species;[43,48] however, in the reaction discussed in this paper, the Mo oxide nanoclusters residing in lattice defects on the zeolite's outer surface are considered the active species.

This study investigated reactions for the production of BTEX from polycyclic aromatic hydrocarbons, including tetralin, 1-MN, naphthalene, and phenanthrene. We have previously reported the conversion of tetralin using acid zeolite, but the BTEX yield was only 20%.[27] Screening of metal species showed that Mo was the only one that improved the BTEX yield (Fig. 7). The Mo loading improved the BTEX yield, while the yields of naphthalene and methylindane decreased; however, in 20-Mo, the BTEX yield decreased due to excessive Mo loading (Fig. 8(a)). The

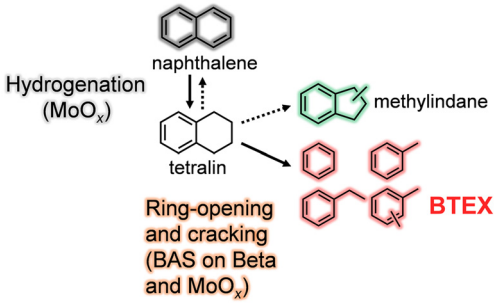

Fig. 9 The role of catalysts in reaction pathways.

reaction order with respect to H_2 pressure was higher on 10-Mo than on 1-Mo (Fig. 8(b)), indicating that H_2 and Mo oxide nanoclusters strongly influence the rate-limiting step in BTEX production from tetralin. It is suggested that the activation of H_2 molecules by the Mo oxide nanoclusters contributed to the improved yield. The following speculation can be made. After the cleavage of the naphthene ring of tetralin by the addition of a proton from BAS on beta zeolite, the addition of hydride from Mo oxide suppressed ring contraction into methylindane, and the ring-opening and cracking formed BTEX (Fig. 9). Our hypothesis is that hydrogen molecules undergo heterolytic cleavage on the Mo oxide, and the resulting hydrogen atoms moves through the zeolite pores to react with the activated tetralin intermediate on the BAS. The heterolytic cleavage of H_2 on metal oxides has been reported.[49] However, as there is no definitive evidence for hydrogen hopping, further research is continued. At low Mo loadings (up to 10 wt%), the reduced Mo primarily exists as MoO_2. However, at higher loadings, the proportion of MoO_2 decreases, while that of Mo^0 increases. An increase in Mo^0 likely reduces the occurrence of heterolytic H_2 cleavage, thereby decreasing the activity of the tetralin conversion. In addition, the dehydrogenation reaction to naphthalene should also be suppressed by the activation of H_2 molecules on Mo nanoclusters. From another perspective, this characteristic is adequate for partial hydrogenation of 1-MN, naphthalene, and phenanthrene. In the 1-MN conversion, beta did not produce BTEX, and isomerization to 2-MN proceeded mainly. On the other hand, BTEX was formed at 10-Mo, indicating that Mo oxide nanoclusters catalyzed the partial hydrogenation of 1-MN and the ring-opening of tetralin. The nanoclusters on 10-Mo with an average valence of approximately +4 are presumably responsible for the reaction. In the mixture of naphthalene and 1-MN under the same reaction conditions, the BTEX yield decreased compared to the case of only 1-MN, but increasing the hydrogen pressure increased the BTEX yield to 52.8 C-mol%. Most of the other products were gaseous products formed from the fragmentation of tetralin, along with BTEX. Finally, the reaction substrate was changed from naphthalene to tricyclic phenanthrene, but the BTEX yield decreased significantly. Since the maximum pressure at which the reaction can be performed safely is 5 MPa, it was not possible to investigate the effect of hydrogen pressure. However, the results so far suggest that BTEX can be produced even with tricyclic aromatic hydrocarbons. It is assumed that dicyclic and tricyclic aromatic hydrocarbons undergo partial hydrogenation upon initial contact with Mo nanoclusters, and the resulting naphthenic products diffuse to the acid sites of beta zeolite, where BTEX is formed. One reason for the decrease in phenanthrene activity is likely diffusion-rate limitation due to its larger molecular size. This study is the first paper to clarify the active catalyst structure and mechanism of a catalyst combining Mo and beta zeolite that produces a high yield of BTEX from polycyclic aromatic hydrocarbons. It is hoped that this paper will serve as a starting point for further research on the conversion of polycyclic aromatic hydrocarbons.

5. Conclusions

This study establishes that Mo oxide nanoclusters-loaded beta zeolite is an effective non-precious-metal catalyst for converting polycyclic aromatic hydrocarbons into valuable monoaromatic hydrocarbons (BTEX) through a synergistic combination of partial hydrogenation and acid-catalyzed ring-opening. Structural characterization revealed that, at optimal Mo loading (around 10 wt%), MoO_x nanoclusters located predominantly at external defect sites on beta zeolite activate H_2 molecules. The strong Brønsted acid sites of the beta zeolite and Mo oxide promoted selective ring-opening. This cooperative function significantly enhances BTEX yield while suppressing side reactions such as ring contraction and dehydrogenation. Catalytic reactions demonstrated that the system achieves up to 62.0 C-mol% BTEX yield from tetralin and 52.8 C-mol% from the mixture of 1-methylnaphthalene and naphthalene under optimized hydrogen pressures, outperforming bare beta zeolite. While phenanthrene conversion was less efficient, the results indicate the feasibility of converting tricyclic aromatics under improved reaction conditions. Overall, this work provides the first mechanistic insight into MoO_x nanocluster-loaded beta zeolite catalysis for high-yield BTEX production from polycyclic aromatic hydrocarbons, offering a promising pathway toward more efficient utilization of heavy petroleum fractions and advancing the development of efficient aromatic hydrocarbon production processes.

Conflicts of interest

The authors declare no conflict of interest.

Data availability

The data supporting this article has been included as part of the supplementary information (SI) and is also available upon reasonable request.

Supplementary information is available. See DOI: https://doi.org/10.1039/d5cy01293g.

Acknowledgements

This work was mainly supported by part of the Projects for Technological Development entrusted by the Ministry of Economy, Trade and Industry, Japan, to the Japan Petroleum Energy Center. The other part was supported by JSPS KAKENHI Grant Number 16H04568, the Japan Petroleum Institute, and the Cooperative Research Program of Institute for Catalysis, Hokkaido University (Proposal #20B1039).

References

1 R. Sahu, B. J. Song, J. S. Im, Y.-P. Jeon and C. W. Lee, *J. Ind. Eng. Chem.*, 2015, **27**, 12–24.
2 S. Mehla, S. Kukade, P. Kumar, P. V. C. Rao, G. Sriganesh and R. Ravishankar, *Fuel*, 2019, **242**, 487–495.
3 E. T. Vogt and B. M. Weckhuysen, *Chem. Soc. Rev.*, 2015, **44**, 7342–7370.
4 G. C. Laredo, P. Pérez-Romo, J. Escobar, J. L. Garcia-Gutierrez and P. M. Vega-Merino, *Ind. Eng. Chem. Res.*, 2017, **56**, 10939–10948.
5 M. Anilkumar, N. Loke, V. Patil, R. Panday and S. G, *Catal. Today*, 2020, **358**, 221–227.
6 N. Katada, Y. Kawaguchi, K. Takeda, T. Matsuoka, N. Uozumi, K. Kanai, S. Fujiwara, K. Kinugasa, K. Nakamura, S. Suganuma and M. Nanjo, *Appl. Catal., A*, 2017, **530**, 93–101.
7 K. Kinugasa, F. Nakano, S. Nagano, S. Suganuma, E. Tsuji and N. Katada, *Sekiyu Gakkaishi*, 2018, **61**, 294–301.
8 S. Suganuma, K. Arita, F. Nakano, E. Tsuji and N. Katada, *Fuel*, 2020, **266**, 117055.
9 F. Nakano, T. Goma, S. Suganuma, E. Tsuji and N. Katada, *Catal. Sci. Technol.*, 2021, **11**, 239–249.
10 G.-N. Yun and Y.-K. Lee, *Appl. Catal., B*, 2014, **150-151**, 647–655.
11 J.-I. Park, S. A. Ali, K. Alhooshani, N. Azizi, J. Miyawaki, T. Kim, Y. Lee, H.-S. Kim, S.-H. Yoon and I. Mochida, *J. Ind. Eng. Chem.*, 2013, **19**, 627–632.
12 Y.-S. Kim, G.-N. Yun and Y.-K. Lee, *Catal. Commun.*, 2014, **45**, 133–138.
13 J.-I. Park, J.-K. Lee, J. Miyawaki, Y.-K. Kim, S.-H. Yoon and I. Mochida, *Fuel*, 2011, **90**, 182–189.
14 Y.-S. Kim, K.-S. Cho and Y.-K. Lee, *J. Catal.*, 2017, **351**, 67–78.
15 L. Yu, H. Nie, P. Yang, L. Wang, S. Feng, H. Gao and G. Wang, *Coord. Chem. Rev.*, 2025, **529**, 216444.
16 M. Usman, D. Li, R. Razzaq, U. Latif, O. Muraza, Z. H. Yamani, B. A. Al-Maythalony, C. Li and S. Zhang, *J. Environ. Chem. Eng.*, 2018, **6**, 4525–4530.
17 M. Usman, D. Li, R. Razzaq, M. Yaseen, C. Li and S. Zhang, *J. Ind. Eng. Chem.*, 2015, **23**, 21–26.
18 S. J. Ardakani and K. J. Smith, *Appl. Catal., A*, 2011, **403**, 36–47.
19 M. Pang, X. Wang, W. Xia, M. Muhler and C. Liang, *Ind. Eng. Chem. Res.*, 2013, **52**, 4564–4571.
20 X. Liu and K. J. Smith, *Appl. Catal., A*, 2008, **335**, 230–240.
21 Y. Choi, J. Lee, J. Shin, S. Lee, D. Kim and J. K. Lee, *Appl. Catal., A*, 2015, **492**, 140–150.
22 M. Pang, C. Liu, W. Xia, M. Muhler and C. Liang, *Green Chem.*, 2012, **14**, 1272–1276.
23 M. Santikunaporn, J. Herrera, S. Jongpatiwut, D. Resasco, W. Alvarez and E. Sughrue, *J. Catal.*, 2004, **228**, 100–113.
24 G. C. Laredo, P. Pérez-Romo, P. M. Vega-Merino, E. Arzate-Barbosa, A. García-López, R. Agueda-Rangel and V. H. Martínez-Moreno, *Appl. Petrochem. Res.*, 2019, **9**, 185–198.
25 A. Kostyniuk, D. Bajec and B. Likozar, *J. Ind. Eng. Chem.*, 2021, **96**, 130–143.
26 J. Qi, Y. Guo, H. Jia, B. Fan, H. Gao, B. Qin, J. Ma, Y. Du and R. Li, *Fuel Process. Technol.*, 2023, **240**, 107586.
27 K. Nakajima, S. Suganuma, E. Tsuji and N. Katada, *React. Chem. Eng.*, 2020, **5**, 1272–1280.
28 S.-U. Lee, Y.-J. Lee, J.-R. Kim and S.-Y. Jeong, *J. Ind. Eng. Chem.*, 2018, **66**, 279–287.
29 Y. Zheng, Y. Tang, J. R. Gallagher, J. Gao, J. T. Miller, I. E. Wachs and S. G. Podkolzin, *J. Phys. Chem. C*, 2019, **123**, 22281–22292.
30 N.-Y. Yao, J.-P. Cao, X.-Y. Zhao, X.-B. Pang, J.-P. Zhao, C.-X. Chen, S.-J. Cai, X.-B. Feng and D. Dung Le, *J. Anal. Appl. Pyrolysis*, 2024, **179**, 106516.
31 M. Niwa and N. Katada, *Chem. Rec.*, 2013, **13**, 432–455.
32 S. Suganuma, K. Nakamura, A. Okuda and N. Katada, *Mol. Catal.*, 2017, **435**, 110–117.
33 M. Renteria, A. Traverse, O. A. Anunziata, E. J. Lede, L. Pierella and F. G. Requejo, *J. Synchrotron Radiat.*, 2001, **8**, 631–633.
34 F. Chen, X.-B. Feng, L.-Y. Zhang, J.-P. Zhao, Z.-M. He, F.-J. Yi, X.-Y. Zhao and J.-P. Cao, *Chem. Eng. Sci.*, 2022, **263**, 118121.
35 L. Qi, C. Peng, Z. Cheng and Z. Zhou, *Fuel*, 2023, **351**, 128941.
36 K. S. W. S. Sing, D. H. Everett, R. A. W. Haul, L. Moscou, R. A. Pierotti, J. Rouquerol and T. Siemieniewska, *Pure Appl. Chem.*, 1985, **57**, 603–619.
37 A. A. Gabrienko, I. G. Danilova, S. S. Arzumanov, A. V. Toktarev, D. Freude and A. G. Stepanov, *Microporous Mesoporous Mater.*, 2010, **131**, 210–216.
38 L. Qi, Y. Zhang, M. A. Conrad, C. K. Russell, J. Miller and A. T. Bell, *J. Am. Chem. Soc.*, 2020, **142**, 14674–14687.
39 T. Kitano, S. Okazaki, T. Shishido, K. Teramura and T. Tanaka, *J. Mol. Catal. A: Chem.*, 2013, **371**, 21–28.
40 K. Amakawa, Y. Wang, J. Kröhnert, R. Schlögl and A. Trunschke, *Mol. Catal.*, 2019, **478**, 110580.
41 I. Lezcano-Gonzalez, R. Oord, M. Rovezzi, P. Glatzel, S. W. Botchway, B. M. Weckhuysen and A. M. Beale, *Angew. Chem., Int. Ed.*, 2016, **55**, 5215–5219.
42 M. Agote-Arán, A. B. Kroner, H. U. Islam, W. A. Sławiński, D. S. Wragg, I. Lezcano-González and A. M. Beale, *ChemCatChem*, 2018, **11**, 473–480.
43 D. Zhou, Y. Zhang, H. Zhu, D. Ma and X. Bao, *J. Phys. Chem. C*, 2007, **111**, 2081–2091.
44 S. Bo, H. Lin, J. Zhang, W. Liao, K. Yang, T. Su, H. Lü and Z. Zhu, *Green Chem.*, 2024, **26**, 2661–2672.

45 S. Rajagopal, J. A. Marzari and R. Miranda, *J. Catal.*, 1995, **151**, 192–203.
46 O. G. Marin Flores and S. Ha, *Appl. Catal., A*, 2009, **352**, 124–132.
47 C. Zhang, J. Lu, M. Li, Y. Wang, Z. Zhang, H. Chen and F. Wang, *Green Chem.*, 2016, **18**, 2435–2442.
48 Y. Okamoto, N. Oshima, Y. Kobayashi, O. Terasaki, T. Kodaira and T. Kubota, *Phys. Chem. Chem. Phys.*, 2002, **4**, 2852–2862.
49 I. Cano, L. M. Martínez-Prieto and P. W. N. M. van Leeuwen, *Catal. Sci. Technol.*, 2021, **11**, 1157–1185.